ARTICLE Communicated by J. van Hateren

The Minimal Local-Asperity Hypothesis of Early Retinal Lateral Inhibition

Rosario M. Balboa
Norberto M. Grzywacz
Smith-Kettlewell Eye Research Institute, San Francisco, CA 94115-1813, U.S.A.

Recently we found that the theories related to information theory existent in the literature cannot explain the behavior of the extent of the lateral inhibition mediated by retinal horizontal cells as a function of background light intensity. These theories can explain the fall of the extent from intermediate to high intensities, but not its rise from dim to intermediate intensities. We propose an alternate hypothesis that accounts for the extent's bell-shape behavior. This hypothesis proposes that the lateral-inhibition adaptation in the early retina is part of a system to extract several image attributes, such as occlusion borders and contrast. To do so, this system would use prior probabilistic knowledge about the biological processing and relevant statistics in natural images. A key novel statistic used here is the probability of the presence of an occlusion border as a function of local contrast. Using this probabilistic knowledge, the retina would optimize the spatial profile of lateral inhibition to minimize attribute-extraction error. The two significant errors that this minimization process must reduce are due to the quantal noise in photoreceptors and the straddling of occlusion borders by lateral inhibition.

1 Introduction

Theories for lateral inhibition existent in the literature that are based on information-theory-like ideas[1] are not consistent with the behavior of lateral inhibition in the retina's outer plexiform layer (OPL) (Balboa & Grzywacz, 2000). These theories can only explain qualitatively the fall of the lateral-inhibition extent as a function of intensity beginning at intermediate intensities (Baldridge & Ball, 1991; Myhr, Dong, & McReynolds, 1994; Lankheet, Rowe, Van Wezel, & van der Grind, 1996). To account for this intensity behavior, three of these theories use second-order statistics (autocorrelation or power spectrum) in natural images (Srinivasan, Laughlin, & Dubs, 1982;

[1] We call these theories information-theory-like, because although they essentially deal with signal-to-noise ratio, as does conventional information theory, they do not quantify information per se, as theory does.

Atick & Redlich, 1992; McCarthy & Owen, 1996), while the fourth (Field, 1994) uses a four-order statistic (the image kurtosis). These theories explain this behavior, because as intensity decreases, the relative noise due to random photon absorption increases. Hence, the theories must increase the lateral-inhibition extent to average out the noise.

No one can rule out that some of the computations performed in the OPL are related to the statistics used by these theories. However, there is something missing to explain the increase of the extent of the OPL's lateral inhibition with intensity at low intensities (Mangel & Dowling, 1985; Baldridge, 1993; Jamieson, 1994; Xin, Bloomfield, & Persky, 1994). The complete behavior from low to high intensities was only recently published (Xin & Bloomfield, 1999); Figure 1 shows this behavior. (Previous experiments were not sufficiently broad to cover carefully the full range of intensities, eliminating artifacts due to adaptation to the test stimuli.) The upper panel shows the electrophysiological measurements of the horizontal cells' receptive-field sizes for two different cell types in the rabbit's retina. The lower panel shows the extension of the neurobiotin coupling for the same horizontal-cell classes. In both panels, the extent is small at low intensities, grows with intensity up to a maximum, and then falls as the intensity increases further. This same intensity behavior was also observed in goldfish (Jamieson, Baldridge, & Ball, 1994). From these results, one can see that different experiments in different species lead to the same bell-shape behavior for horizontal cells and, thus quite likely, for the lateral inhibition that they mediate. Moreover, given that it was observed in different types of horizontal cells, one can say that this is a general behavior, which is not explained by previous theories.

In this work, we propose a new information-theory-like hypothesis for the role of the OPL's lateral inhibition. We focus on the OPL, because it is the first stage of visual processing and therefore must be dealing with general aspects of natural images. The new hypothesis will be shown to be consistent with the OPL's intensity behavior. Relatedly, the hypothesis can account for the disappearance of lateral inhibition at extremely low intensities (Barlow, Fitzhugh, & Kuffler, 1957; Bowling, 1980) and the shrinkage of its extent for stimuli that are not spatially homogeneous (Reifsnider & Tranchina, 1995; Kamermans, Haak, Habraken, & Spekreijse, 1996). Moreover, the hypothesis explains the inhibition's division-like mechanism of action (Merwine, Amthor, & Grzywacz, 1995; Verweij, Kamermans, & Spekreijse, 1996) and linearity under low contrasts (Tranchina, Gordon, Shapley, & Toyoda, 1981). Finally, the hypothesis is consistent with the psychophysics of the Steven's power law of intensity perception (Stevens, 1970) and the asymmetry of positive and negative Mach bands at the two sides of an intensity border (Fiorentini & Radici, 1957; Ratliff, 1965). The hypothesis and its predictions have already appeared in abstract form (Balboa & Grzywacz, 1998).

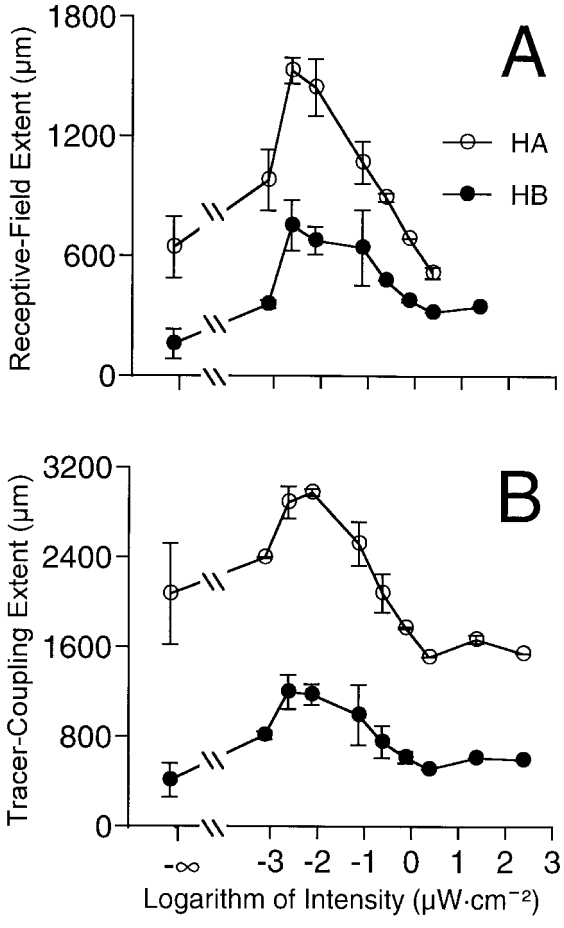

Figure 1: (A) Electrophysiological receptive-field-extent measurements for two different types of horizontal cells in the rabbit retina: type A (HA; empty circles) and type B (HB; filled circles). When dark adapted ($-\infty$), the receptive-field extent is small. It then rises with background intensity up to a maximum and falls again as the intensity continues to increase. (B) Tracer-coupling extent with neurobiotin in the same cell types. The coupling has the same behavior as the receptive fields in A. (Data from Xin & Bloomfield, 1999.)

2 Hypothesis Rationale

2.1 Philosophy. There is a major philosophical difference between the new hypothesis and some of the theories in the literature (Atick & Redlich, 1992; McCarthy & Owen, 1996). Past theories prescribe extracting the largest

amount possible of nonredundant signal. The new hypothesis prescribes extracting as well as possible signal that is relevant for the animal. An example of what we mean by "relevant" is provided by the work of Kamermans and colleagues with the goldfish's OPL (Kamermans, Kraaij, & Spekreijse, 1998). If it were to extract all the color information from the scene, then it should obtain information about the color of the objects and illuminant. However, the goldfish's OPL appears to discard, or at least pay much less attention to, the illuminant's color. Why would the visual system play down some types of information so early in the processing? We propose two answers to this question. First, by devoting the available output channels of information to fewer types of signal, larger quantities of these signals can be transmitted. Second, if one assumes that the central nervous system has limited capacity, then the system might be better off dealing with fewer types of signal than by dividing its energy among many types, some of which may not be relevant for the animal's survival.

What types of signal should lateral inhibition play down or stress? The most obvious type is illumination. For example, the predictive coding theory (Srinivasan et al., 1982) proposes to reduce information about the intensity of illumination of points whose neighbors have the same intensity. The goal is to fit the wide range of intensities in natural scenes in the narrow dynamic range of the second-order neuron, for instance, the bipolar cell. However, the retina must achieve this goal before lateral inhibition, since the photoreceptor itself has a narrow dynamic range (Fain & Dowling, 1973; Baylor, Lamb, & Yau, 1979). Hence, different from the predictive coding theory, we suggest that the main goal of lateral inhibition is not codification of intensity.

Rather, we propose that the nonchromatic goals of the OPL's lateral inhibition are to aid in the optimization of border detection (Shapley & Tolhurst, 1973), and contrast (Campbell & Robson, 1968) and intensity (Stevens, 1970) estimation. Contrast would be particularly important at borders, and intensity would be important away from them. Border position is an important piece of information, because it is from it that the visual system would characterize objects. As such, lateral inhibition is the first step of image segmentation, by being the first step of edge detection. Because we emphasize object segmentation, we place particular importance on occluding edges. However, this does not mean that we think that the retina discriminates different types of edges (such as occlusions and shadows). Edge discrimination requires relatively high-level cues (Adelson 1993; Wishart, Frisby, & Buckley, 1997) beyond the scope of the retina. All that we are proposing is that the retina contributes directly to border extraction, with the retinal circuitries designed specifically to deal with the statistics of occluding borders. The idea of lateral inhibition being important for border extraction is not new (Ratliff, 1965). What is new here is quantifying the cost of missing borders and specifying the information obtained from them and away from them.

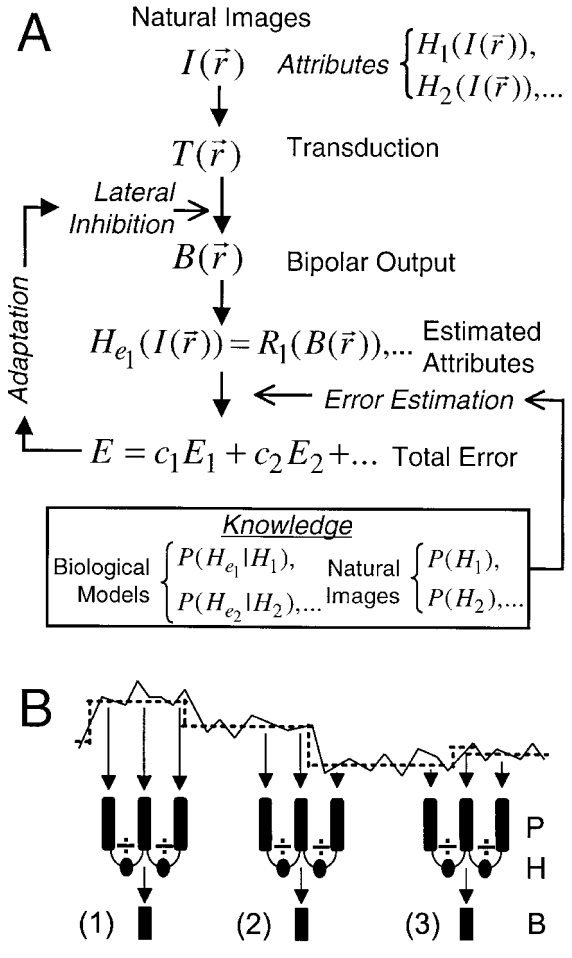

2.2 Lateral Inhibition and Image-Attribute Extraction. Figure 2.2A illustrates the structure of the new hypothesis for lateral inhibition as a process in the extraction of image attributes. From the stimulus ($I(\vec{r}\,)$, where $\vec{r}$ is position), the retina wishes to estimate a few attributes (the functions $H_1, H_2, \ldots$), particularly the position and contrast of edges and the intensity outside edges. To do so, it first transduces the stimulus through a noisy process, getting the photoreceptor responses ($T(\vec{r}\,)$). Then lateral inhibition modulates these responses, giving rise to bipolar responses ($B(\vec{r}\,)$). Consider the spatial layout of these responses across the population of the bipolar cells. Wherever there are edges in the image, there are fluctuations in the layout caused by the lateral inhibition—the so-called Mach bands (Ratliff,

1965). The contrast of an edge and its Mach band's amplitude (or largest spatial gradient) is linearly related. Because the probability that there is an edge due to occlusions in a point of the image increases with the contrast at that point (Balboa & Grzywacz, 1999c), the spatial bipolar gradient of any given point codes the probability that there is an edge there. Therefore, for a point in the image with a high spatial gradient across bipolar cells, the position of these cells indicates the position of a likely edge, and the gradient is proportional to the presumed edge's contrast. For points with low gradient, the bipolar cells would code an amplitude-compressed representation of $T(\vec{r})$. We propose that the visual system implements recovery functions ($R_1(B(\vec{r}))$, $R_2(B(\vec{r}))$, ...) to go from the bipolar responses to estimates (H_{e_1}, H_{e_2}, ...) of the image attributes. For each attribute, the visual system computes the expected error (E_1, E_2, ...) by taking into account the prior probability of the attribute in natural images ($P(H_1)$, $P(H_2)$, ...), the probabilistic model relating the attribute to the estimate ($P(H_{e_1}|H_1)$, $P(H_{e_2}|H_2)$, ...), and Bayesian theory. These models and prior probabilities would come from learning during development or evolution. The models amount to knowledge about the biology linking the stimulus to the estimates of the attributes. The prior probabilities amount to knowledge of the attributes in natural images.

The new hypothesis postulates that the profile of lateral inhibition changes to minimize the total error, that is,

$$E = C_1E_1 + C_2E_2 + \cdots, \tag{2.1}$$

Figure 2: *Facing page*. Rationale of the minimal-local asperity hypothesis. (A) Schematics of the hypothesis. Images are transduced and transformed to bipolar cell output with the participation of lateral inhibition. Several recovery functions (R_1, R_2, ...) implemented neurally transform the bipolar output to a new signal (H_{e_1}, H_{e_2}, ...), which represents estimates of desired attributes from the image (H_1, H_2, ...). The system then computes the estimation error by using prior knowledge about images and the underlying biology. A signal representing the error feeds back to the OPL to modulate lateral inhibition. (B) Schematics of stimuli and OPL. The dashed line represents the intensities of objects in the world, while the solid line adds the quantal noise to these intensities. Photoreceptors (whose responses are the solid lines) and horizontal and bipolar cells are represented by the shapes labeled P, H, and B, respectively. The figure uses three labeled sites to illustrate three cases of the relationship between these cells and the stimulus. In site 1, the lateral inhibition mediated by the horizontal cells is confined to one object, helping to compress its intensity to the neural signal. This signal suffers from the quantal-noise error. In site 2, the local circuit straddles one border, producing a Mach band signal, which helps to code the border's location and contrast. Finally, in site 3, lateral inhibition straddles more than one border, leading to an erroneous border-detection process (the local-asperity error).

where the C_i's are constants, which weigh the cost associated with each error. They are inversely related to "fitness" in population genetics[2] (Ridley, 1993) and directly related to the "loss function" in economics (Berger, 1985) and computer science (Gallant, 1995).

Figure 2.2B is a one-dimensional (1D) scheme, which illustrates what the main errors in the estimation of the desired visual attributes are. This scheme shows the intensity levels of five 1D objects (dashed line), with the photon-absorption noise superimposed (solid line). Lateral inhibition mediated by horizontal cells (H) acts directly on the photoreceptors (P), modulating their intensity estimate before it reaches the bipolar cell (B). For reasons of clarity, we show only three nonoverlapping sites of lateral inhibition to describe the dominant errors. Depending on the site, what would the response of the bipolar cell be? In site 1, the bipolar response would provide an estimate of the intensity inside the object. The only error in this site would be due to the photon-absorption noise. In site 2, the bipolar cell and its neighbors would be coding something like the position of a border and its contrast. Again, the main source of error for contrast estimation is the photon-absorption noise. In site 3, the borders of the small object might be altogether missed, since the bipolar cell would be receiving inputs related to three different objects, corrupting its signals. Consequently, there are two dominant sources of errors: the photon-absorption noise and the straddling of multiple borders by lateral inhibition. We call the errors due to the first source the quantal-noise errors and the error due to the second source the local-asperity error. (*Asperity* means "roughness of a surface." If one thinks of images as three-dimensional representations of the intensities in each point, then an asperous image would have a harsh profile.)

2.3 Lateral-Inhibition Extent. The spatial extent of the inhibitory filter is designed to minimize the error in equation 2.1 given a model like that in Figure 2.2A. Mathematical analysis confirms that the two dominant sources of errors are those illustrated in Figure 2.2B (see section 3.2). Theories in the literature all take into account the quantal-noise error (Rushton, 1961). Its process is well known, and the probability of photon absorption follows a Poisson distribution (Fuortes & Yeandle, 1964; Baylor et al., 1979; Grzywacz, Hillman, & Knight, 1988). We estimate the error of this process (section 3) as a function of intensity and the extent of the lateral-inhibition filter. Reducing the intensity produces a relatively noisier signal. To compensate for the error being larger, the system should average the signal over a wider sample of photoreceptor responses and therefore increase the

[2] Population genetics quantifies the evolution of a population of certain genes, starting from their initial frequencies, and how fit they are for reproduction and survival. In our case, the measure of "fitness" is related to the contribution of visual behavior to these genes' success.

extent of the lateral-inhibition filter. The problem with such an average is that more borders would be straddled, causing the local-asperity error. Hence, ideally, to minimize the local-asperity error, the retina would have to use narrow lateral-inhibition extents. It follows that the quantal-Noise and local-asperity errors impose opposite demands on lateral inhibition. To alleviate this problem, the minimal local-asperity hypothesis proposes that the retina chooses the extent of lateral inhibition to minimize a weighed sum of these errors (see equation 2.1), that is, that the retina reaches a compromise.

2.4 Lateral Inhibition's Mechanism. We chose a division-like mechanism of lateral inhibition to implement the hypothesis. In other words, the inhibition corresponds not to the subtraction of the signal from the surround (as in a difference of gaussians model; Rodiek & Stone, 1965) but rather to a division (reduction of gain) of the center's signal. We chose this form of inhibition for three reasons. First, it would be useful to maintain intensity information for regions away from borders. A division-like inhibition ensures the maintenance of this information, whereas a subtractive inhibition may not (Srinivasan et al., 1982). Second, mathematical analyses of subtractive and division-like models (Grzywacz & Balboa, 1999) reveal that the latter but not former allows the extraction of contrast locally. In the linear model, a bipolar cell's signals confound contrast, mean intensity, and amplitude of inhibition. The only way to disambiguate these signals is to obtain global information about the mean intensity. Third, biophysical evidence points out that the OPL's lateral inhibition works through a Ca^{2+}-dependent Cl^{-} conductance at the photoreceptors synapse (Verweij, Kamermans, & Spekreijse, 1996). Such a conductance operates in a division-like manner.

3 Mathematical Formulation

3.1 Lateral Inhibition's Mechanism. Let the intensity-dependent input and output to the photoreceptor's synapse at position (i, j) be $T'_{i,j}$ and $B_{i,j}$, respectively. One can think of $T'_{i,j}$ as the current generated by transduction and $B_{i,j}$ as the voltage at the bipolar cell or presynaptic site. (The variable B_{ij} can be pre- or postsynaptic, since we assume here for simplicity that the synapse is linear, but our arguments do not depend on that.) The output is

$$B_{ij} = \frac{T'_{ij}}{g'_r + g'_I}, \tag{3.1}$$

where $g'_r > 0$ is inversely proportional to the resting gain of the photoreceptor's synapse (the resting conductance) and g'_I is inversely proportional to the gain change due to lateral inhibition (varying conductance). (For the justification of using a division-like inhibition, see the text following

equation 2.1.) Next, we simplify this equation by dividing the numerator and denominator by g'_r, and defining $T_{ij} = T'_{ij}/g'_r$ and $g_I = g'_I/g'_r$. We propose to set $g_I = (h_{i,j} * B_{i,j})^n$, where $*$ stands for convolution, $h_{i,j} \geq 0$ is the lateral-inhibition filter, and $n \geq 1$ is a constant. From this proposition and equation 3.1, we have

$$B_{i,j} = \frac{T_{i,j}}{1 + (h_{i,j} * B_{i,j})^n} . \tag{3.2}$$

That this equation uses a convolution means that lateral inhibition pools the photoreceptor outputs linearly. It is also imposed for simplicity and because there is no evidence against, that if $i^2 + j^2 = k^2 + l^2$, then $h_{i,j} = h_{k,l}$, that is, the inhibitory filter is isotropic. Finally, that equation 3.1 raises $h_{i,j} * B_{i,j}$ to the power of n could mean the cooperation of n molecules of inhibitory transmitter or, nonexclusively, nonlinearities in the calcium or chloride conductances.

3.2 Lateral Inhibition's Extent. The goal is to find the lateral-inhibition filter that minimizes the error in equation 2.1 in a model like that in Figure 2.2. Elsewhere (Grzywacz & Balboa, 1999), we performed a mathematical analysis to estimate this error. The results of the analysis are similar to the intuition provided in Figure 2.2B, which shows that formulas for errors similar to those presented below are expected from models like that in Figure 2.2A no matter what approximations one uses. Briefly, the analysis used the following mathematical procedures: Errors were typically quantified as spatial integrals of the square of the relative differences between desired attributes and their estimates. We used a Bayesian formulation to weigh the various possible images and the estimated attributes from these images. For this purpose, it was assumed that the attribute estimation from a given image was corrupted by Poisson noise. We then linearized the errors with Taylor expansions around the mean intensity, assuming that the images did not have intensities that were too low (relatively little noise) and contrasts that were too high (Ruderman & Bialek, 1994; Vu, McCarthy, & Owen, 1997; Zhu & Mumford, 1997; Balboa & Grzywacz, 1999b). Finally, it was assumed that the width of inhibitory filter is much narrower than the mean size of objects in the images, making simultaneous crossing of two borders when centering the filter on a point rare but not impossible. This was a simplifying assumption that was probably at best rough for "cluttered" images (Zhu & Mumford, 1998). However, this assumption probably held for most images, since the receptive fields of retinal cells are typically narrow. This assumption allowed approximating the number of local-asperity errors (multiple-border crossings) as a Poisson distribution (large number of positions and low probability of crossings). After this analysis, a good

approximation for the error (see equation 2.1) was

$$E = E_Q + E_A, \tag{3.3}$$

where E_Q and E_A are the quantal-noise and local-asperity errors, respectively. (Compared to equation 2.1, equation 3.3 arbitrarily left out the C_i coefficients, because E_Q and E_A have free, multiplicative gain parameters.)

The analysis (Grzywacz & Balboa, 1999) also revealed that the quantal-noise error is to a good approximation

$$E_Q = \frac{\varphi_Q \left(\sum_i \sum_j \hat{h}_{i,j}^2 \right)^{1/2}}{\langle I_{i,j} \rangle^{1/2}}, \tag{3.4}$$

where $\varphi_Q > 0$ is a free parameter of the hypothesis, $\hat{h}_{i,j} = h_{i,j} / \sum_{i,j} h_{i,j}$ is the filter normalized, and $\langle I_{i,j} \rangle$ is the mean input to the photoreceptor's synapse from the photoreceptor's outer segment averaged over all positions (i, j). Although we do not derive this equation here, understanding its interpretation will help clarify its appropriateness.

The equation's parameter φ_Q indicates the noisiness of the photoreceptors. The quantal noisiness varies with the amplitude and time course of the single-photon response (Fuortes & Yeandle, 1964; Lillywhite, 1977; Baylor et al., 1979; Grzywacz et al., 1988), and thus, φ_Q has a wide range of values in nature. Expectedly, as the noisiness increases, the quantal-noise error (E_Q) becomes larger. Also as expected, the quantal-noise error falls with the square root of the input. This is because the quantal-noise error is a relative error and the noise (standard deviation)-to-signal (mean) ratio in a Poisson process is inversely proportional to the square root of the signal (Burington, 1973). Finally, the error in equation 3.4 can be reduced by changing $\hat{h}_{i,j}$. As $\hat{h}_{i,j}$ becomes more spatially extended, its values become smaller, since $\sum_{i,j} \hat{h}_{i,j} = 1$ and $\hat{h}_{i,j} \leq 1$ (since $h_{i,j} \geq 0$). This causes $\hat{h}_{i,j}^2$ to fall rapidly, reducing $\sum_{i,j} \hat{h}_{i,j}^2$ and thus E_Q. In other words, the larger the spatial extent of the inhibitory filter ($h_{i,j}$) is, the smaller the quantal-noise error is.

We also analyzed the local-asperity error (E_A in equation 3.3; Grzywacz & Balboa, 1999). Because this error depends on the size of the inhibitory filter, one needs to estimate its width. One example of such an estimate is the spatial standard deviation (ρ) of $\hat{h}_{ij}$. (Because $\sum_{ij} \hat{h}_{ij} = 1$ and $0 \leq \hat{h}_{ij} \leq 1$, $\hat{h}_{ij}$ is a probability function and thus has a well-defined standard deviation.) It should not be surprising that under the assumptions described above, the

local-asperity error is to a good approximation

$$E_A = \varphi_A \sum_k \sum_l \left(\sum_{ij \atop (i-k)^2+(j-l)^2 \le \pi\rho^2} P_O\left(\left| \frac{\nabla I}{I} \right|_{i,j} \right) \right), \tag{3.5}$$

where $\varphi_A > 0$ is a constant and $P_O(|\frac{\nabla I}{I}|_{i,j})$ is the probability that there is an occluding border at position (i, j) given that the contrast there is $|\frac{\nabla I}{I}|_{i,j}$ (footnote 3). This equation is proportional to the mean number of occluding borders found when a window of radius ρ is placed over an arbitrary point in the image. The "k" and "l" sums perform calculation of mean over the retina (with the normalization constant included in φ_A). The "i" and "j" sum is proportional (also through φ_A) to the number of borders around position (k, l). This is because P_O gives the probability (fraction) of a border at each position.

Elsewhere (Balboa & Grzywacz, 1999b), we present results of measurements of $P_O(|\nabla I/I|_{i,j})$, which are needed for estimating the local-asperity error through equation 3.5. In that work, we show that one of the main properties of this function is that it is a sigmoidal function of local contrast. Because the vast majority of contrasts are low (Ruderman & Bialek, 1994; Vu et al., 1997; Zhu & Mumford, 1997; Balboa & Grzywacz, 1999b), we here neglect the saturation portion of the sigmoidal and approximate

$$P_O\left(\left| \frac{\nabla I}{I} \right|_{i,j} \right) = \left| \frac{\nabla I}{I} \right|_{i,j}^m, \tag{3.6}$$

where $m \ge 1$. A multiplicative constant that should appear on the right-hand side of this equation is set to 1 without loss of generality, since the balance between E_Q and E_A is controlled by the parameters φ_Q and φ_A (see equations 3.4 and 3.5).

3.3 Lateral Inhibition's Amplitude. Why does the amplitude of h not matter much for the computation of error? Although the lateral-inhibition extent matters for the quantal-noise error, the amplitude of $h_{i,j}$ does not, since equation 3.4 depends only on the filter normalized, $\hat{h}_{i,j}$. (However, this amplitude matters for the OPL's output.) The amplitude is eliminated in the derivation of equation 3.4, since the quantal-noise error is relative, that is, it is standard deviation over mean. Similarly, errors made by the

[3] This is the most natural definition of local contrast for the problem at hand. One thinks of local contrast as the ratio between the difference of intensities in neighbor points and the mean intensity. However, for an image on a continuous domain, neighbor points are not well defined. Therefore, a differential definition of contrast using the gradient operation is natural.

local-asperity term do not depend on h's amplitude. They are just a count of how many multiple borders are crossed on average when centering the filter on a point in the image. This is because the error depends only on the probability that borders pass through points inside the filter, and this probability is independent of the filter's amplitude.

4 Results

4.1 Bell-Shape Behavior. We simulated our hypothesis with 89 natural underwater and atmospheric images collected from the World Wide Web (Balboa, 1997). In the simulations, we found the inhibitory filter that minimized the attribute-estimation error expressed in equation 3.3 using equations 3.4 and 3.5, and the methods in the appendix. The main result of the simulations appears in Figure 3. It reveals a bell-shape behavior of the lateral-inhibition extent as a function of intensity. The rise at low intensities begins at around 3 to 10 photons per integration time of the photoreceptor. Therefore, the hypothesis predicts that the bell-shape behavior is due to cone processing, because rods are saturated at these intensity levels (Rao, Buchsbaum, & Sterling, 1994). This behavior contrasted with that stemming from other theories of lateral inhibition in the literature (Srinivasan et al., 1982; Atick & Redlich, 1992; Field, 1994). Those theories predicted that the lateral-inhibition extent falls with intensity (Balboa & Grzywacz, 2000). The stepwise appearance of this extent as a function of intensity in Figure 3 was due to our searching of the extent of the optimal filter in jumps of powers of 2 (see the appendix). However, averaging the lateral-inhibition extent across images eliminated this stepwise appearance.

Figure 3 also presents the dependence of the bell-shape behavior of the lateral-inhibition extent on φ, which is proportional to the ratio between the weight of the quantal-noise error (φ_Q—see equation 3.4) and that of the local-asperity error (φ_A—see equation 3.5) (see the appendix). The effect of a rise in φ is to increase the lateral-inhibition extent as φ rises. Figure 4 illustrates the effect of the shape of $P_O\left(\left|\frac{\nabla I}{I}\right|_{i,j}\right)$ on the bell-shape curves. The main free parameter quantifying this shape is m, which gives the power of the rise of $P_O\left(\left|\frac{\nabla I}{I}\right|_{i,j}\right)$ as a function of $\left|\frac{\nabla I}{I}\right|$ (see equation 3.6). The effect of this parameter is to increase the lateral-inhibition extent as m rises. Moreover, for small m (little curvature), the new hypothesis no longer predicts a bell-shape behavior but only a fall of the lateral-inhibition extent as a function of intensity. For $m = 1$, there never was a bell-shape behavior; for $m = 2$ this behavior occurred in 80 images out of 89; and for $m = 4$, this behavior was always there.

4.2 Habitats. Besides depending on the hypothesis parameters, the lateral inhibition's bell-shape behavior also depends on the visual habitat.

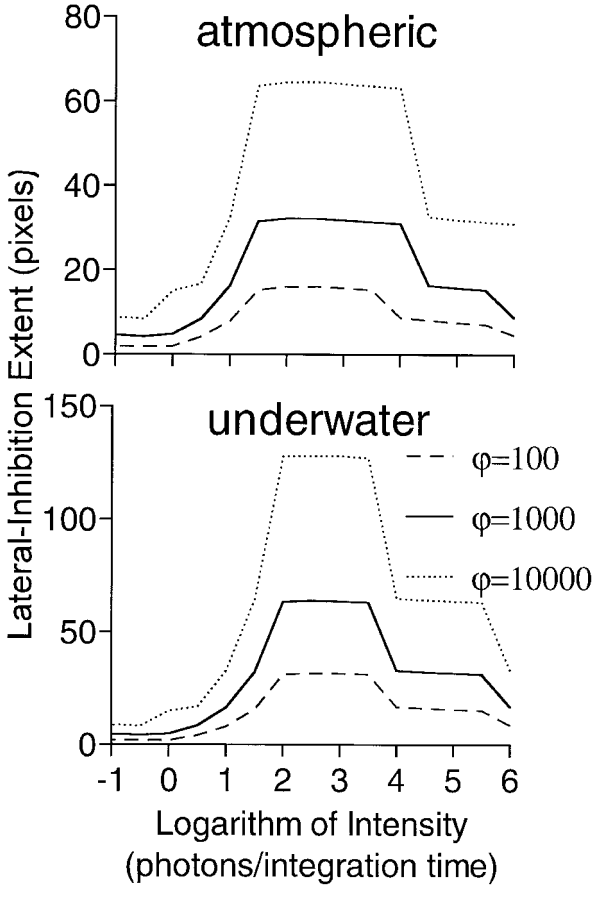

Figure 3: Lateral-inhibition extent as a function of intensity and parametric on φ, which weighs the quantal-noise error relative to the local-asperity error. Standard curve (solid): $\varphi = 1000$, $m = 4$. The other curves vary only φ. There is a bell-shape behavior in the lateral-inhibition extent for the two images shown. By increasing φ, the lateral-inhibition extent increases.

There is a small statistical difference in the lateral-inhibition extent between underwater and atmospheric images (one-sided Mann-Whitney test, $DF = 87, U = 727, z = 2.12, p < 0.0172$). The difference is such that the mean maximal extent of lateral inhibition is 33% larger in underwater than in atmospheric images. One can explain this by observing that light scattering and absorption are so high in water (Mobley, 1995) that underwater images

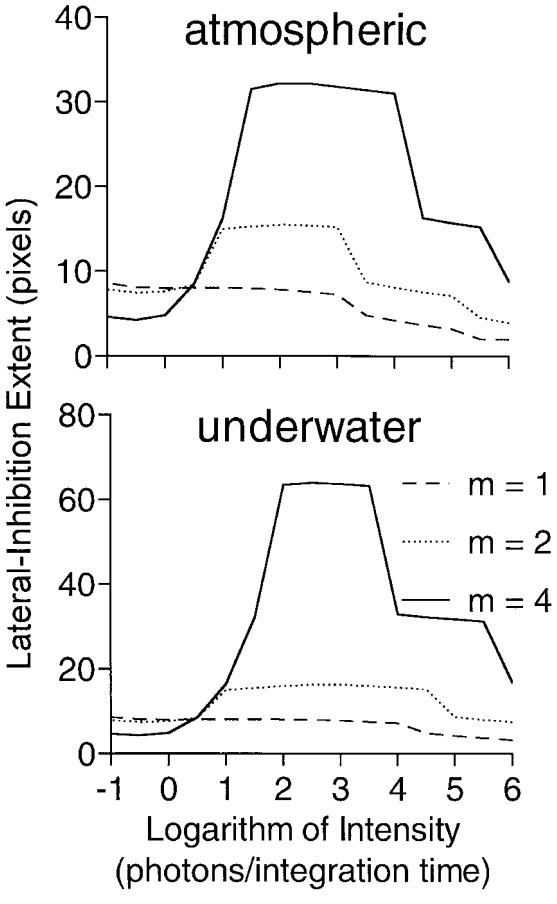

Figure 4: Lateral-inhibition extent as a function of intensity, and parametric on m, which models the curvature of the probability-of-real-borders-as-a-function-of-contrast curve. Standard curve (solid): $\varphi = 1000$, $m = 4$. The other curves vary only m. There is a bell-shape behavior in the lateral inhibition extent for the two images shown, but only when $m > 1$ that is, when there is a curvature in the probability-of-real-borders distribution.

often have large regions of relatively constant intensity. Relatedly, another aspect of visual habitats that seems relevant is whether they have many small objects (as in tropical foliage) or large regions of relatively constant reflectance (as in Arctic scenes). To test whether such habitats lead to different receptive fields according to the minimal-local asperity hypothesis,

we reclassify the images into smooth and rugged categories.[4] The maximal extent of lateral inhibition for smooth images is larger than for rugged images (one-sided Mann-Whitney test, $DF = 34$, $U = 101$, $p < 0.05$). The mean maximal extent was 45% larger for smooth than for rugged images. (Such a difference was observed in horizontal cells when using smooth and rugged backgrounds; Reifsnider & Tranchina, 1995; Kamermans et al., 1998.)

4.3 Other Results Consistent with Biology. As defined in equation 3.2, lateral inhibition would help with luminance adaptation, complementing mechanisms such as pupil-size change and photoreceptor adaptation (for a review see Dowling, 1987). To see this, let $T_{i,j} = T_0$ and $B_{i,j} = B_0$ be constants. (This simplistic example corresponds to a steady-state stimulus with no borders or noise.) Then,

$$B_0 = \frac{T_0}{1 + h_0^n B_0^n}, \tag{4.1}$$

where $h_0 = \sum_{i,j} h_{i,j}$. From this equation one gets

$$B_0 + h_0^n B_0^{n+1} = T_0. \tag{4.2}$$

This equation shows that B_0 grows monotonically with T_0, since

$$\frac{dT_0}{dB_0} = 1 + (n+1)h_0^n B_0^n > 0, \tag{4.3}$$

and that if $T_0 = 0$, then $B_0 = 0$. At low light levels, $B_0 \gg B_0^{n+1}$ (because B_0 grows with T_0 and $B_0(T_0 = 0) = 0$) and therefore,

$$B_0 = T_0. \tag{4.4}$$

Consequently, the response grows proportionally with intensity at low intensities, which is consistent with the biological data (Ashmore & Falk, 1980; Robson & Frishman, 1995). Another biologically correct consequence of $\lim_{T_0 \to 0} B_0 = 0$ is that lateral inhibition disappears at low intensities (Barlow et al., 1957; Bowling, 1980).

[4] Four individuals (two were the authors) performed a classification of all the images according to the following instruction: "We are giving you a set of eighty-nine natural images. Imagine that at each pixel, one inserts a column perpendicular to the plane of the image to a height proportional to the pixel's gray level. This would form a three-dimensional surface. Please classify the images into two sets of approximately equal sizes, such that one set contains those images with the largest regions of relatively low roughness in the imaginary three-dimensional surface." After the individuals performed this classification, we placed into the "smooth" and "rugged" categories only those images that all the individuals judged to have low and high roughnesses, respectively.

At high intensities, $B_0^{n+1} \gg B_0$, and

$$B_0 = \frac{T_0^{\frac{1}{n+1}}}{h_0^{\frac{n}{n+1}}}, \tag{4.5}$$

which, if h_0 does not depend strongly on intensity, corresponds to a strong intensity compression, that is, luminance adaptation. This compression is caused by the division in equation 3.1, not by n, since there is also compression for $n = 1$. However, the compression is stronger when $n > 1$. This compression leads to a power law behavior with intensity, being thus directly consistent with the Stevens's power law (Stevens, 1970). A connection between this law and a similar feedback mechanism was noted previously for invertebrate photoreceptors (Grzywacz & Hillman, 1988). Therefore, one of the roles proposed by the minimal local-asperity hypothesis for lateral inhibition in the OPL is the compression of the wide range of natural intensities into the narrow dynamic range of the bipolar cells (their total range is about 20 mV—Werblin, 1977—and their noise is of the order of 1 mV). This compression should occur in regions of the image away from borders (see Figure 2.2B, site 1). We observe such a compression, which is strengthened as the inhibitory feedback's power (n) increases (see Figure 5). As mentioned before, this form of compression is identical to the Steven's power law (Stevens, 1970). However, observe that there is no compression until on average about one photon is absorbed per integration time of the photoreceptor (see Figure 5).

Besides the bell-shape behavior (see Figures 3 and 4) and the adaptation-related Stevens's power law behavior (see Figure 5), the minimal local-asperity hypothesis is also consistent with at least four other aspects of retinal biology (two of which were discussed above, but are recapitulated here to condense all the biological implications of the hypothesis in a single place). First, at low background intensity, lateral inhibition disappears, as discussed after equation 4.4 (Barlow et al., 1957; Bowling, 1980). Second, the mechanism of action should be division-like, as discussed after equation 2.1 (Merwine et al., 1995; Verweij, Kamermans, & Spekreijse, 1996). Third, the same mathematical analysis that led to equation 3.3 (Grzywacz & Balboa, 1999) shows that despite being division-like, lateral inhibition would lead to responses proportional to contrast even when relatively high gradients of illuminations exist (Tranchina et al., 1981). Fourth, that analysis also shows that positive Mach bands tend to be larger than negative ones, particularly at low background intensities (Fiorentini & Radici, 1957; Ratliff, 1965). An intuition for this asymmetry arises when one considers the extreme case of an edge for which only one of its sides has zero intensity. Because inhibition is division-like, the zero-intensity side will not respond (zero divided by another number is still zero) and thus not develop a Mach band (see equation 3.1), whereas the other side will.

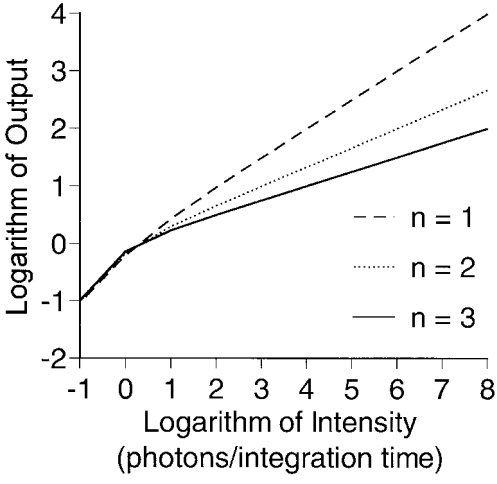

Figure 5: Output at the bipolar cell level as a function of intensity and parametric on n, which models the stoichiometry of the horizontal cell feedback. The units of intensity are arbitrary, since the curves were obtained from equation 4.2 with an arbitrary but constant value of h_0. At low intensities, there is no compression (linear intensity-output relationship; slope = 1), but at higher intensities, there is (sublinear intensity-output relationship; slope < 1). The compression increases with n (lower slopes). In the no-compression regime, lateral inhibition is negligible.

5 Discussion

This article shows that the minimal local-asperity hypothesis can account for the bell-shape behavior with light intensity of the OPL's lateral-inhibition extent (see Figures 3 and 4; Baldridge, 1993; Jamieson, 1994; Xin et al., 1994; Xin & Bloomfield, 1999). Moreover, this hypothesis is consistent with several other physiological- and psychophysical-related behaviors (see section 4.3). A testable prediction of this hypothesis is that the details of the bell-shape behavior will depend on the habitat where the animal lives (see section 4.2). We also studied the role of three independent parameters of the hypothesis: the weight of the quantal-noise error relative to the local-asperity error (see Figure 3), the power of the dependence on contrast of the probability that an occluding border passes through a point (see Figure 4), and the exponential power of the inhibitory action (see Figure 5).

5.1 Limitations. Before embarking on a discussion of the implications of the results, we address some of the limitations of the minimal local-asperity hypothesis. Perhaps the most important variable that this hypothesis did

not consider is time. Adaptation of lateral inhibition must be performed taking into account the different range of visual speeds of different animals and thus possibly different timescales. Therefore, the hypothesis may have to be reformulated to incorporate the animals' speeds. In particular, one may have to study the distribution of occluding borders in images with movement at different speeds (movement may cause border blurring and therefore losses of contrast). Besides movement, another issue that the hypothesis does not address, which is particularly relevant for the OPL, is color processing. This issue may not be major for primates, for which the OPL's lateral inhibition is not color coded (Calkins & Sterling, 1996; Dacey, 1996), but may be key for other vertebrates (Ogden, Mascetti, & Pierantoni, 1985; Ammermüller, Muller, & Kolb, 1995). Teleost fish, for example, have complexly color-coded lateral inhibition mediated by three types of horizontal cells (for a review, see Dowling, 1987). And these fish's lateral inhibition appears to contribute to color constancy, discarding the illuminant information (Kamermans et al., 1998). Hence, it may be simplistic to consider the spatial processing role of lateral inhibition without considering its chromatic one. Verweij, Kamermans, van den Aker, & Spekreijse, (1996) data highlight this conclusion by showing that the receptive field's spatial profiles in the goldfish's outer retina is color dependent. In our defense, we were trying to explain a spatial behavior and succeeded where previous theories failed (Balboa & Grzywacz, 2000). Moreover, the ideas developed here can be extended from the spatial domain to formulate a spatiochromatic version of the minimal local-asperity hypothesis.

Another limitation of the hypothesis comes from a top-down consideration. Estimation of the local-asperity error requires prior knowledge about the probability of occluding borders as a function of contrast in natural images and knowledge about the computations performed by the neural processes involved (see Figure 2.2). Although the hypothesis specifies the type of knowledge needed (probability distributions) and its mode of use (Bayesian estimation), it does not tell how to obtain the information. All we can say is that it should probably come from evolutionary or developmental learning, or both. Studies on the learning of prior distributions are under way in biological and computer vision (Weiss, Edelman, & Fahle, 1993; Zhu & Mumford, 1997; Jones, Sinha, Vetter, & Poggio, 1997; Bartlett & Sejnowski, 1998). Another computationally related limitation is that we implement the hypothesis using individual images, but propose that local asperity is an error learned over many images. The assumption is that an individual image provides a sufficiently rich sample of its habitat. In practice, though, the retina may not make this assumption, pooling a large sample of images to control adaptation. This would explain why the timescale of adaptation is so slow (for a review see Dowling, 1987).

One more limitation that we wish to address has to do with our natural images. The images come from the World Wide Web, and thus lack intensity calibration and may miss energy at high spatial frequencies due

to JPEG (Joint Photographic Experts Group) compression (Fernandez, 1997) and the photographic lens's modulation transfer function (Kodak Professional Photographic Catalog, Kodak, Rochester, NY). We next argue that lack of intensity calibration and high-frequency loss are not serious problems for our results.

To test whether intensity calibration limits our conclusions, we applied the hypothesis to nine calibrated images (Mackeown, 1994) from the Sowerby Image Database (Sowerby Research Centre, British Aerospace). The simulations yielded a bell-shape behavior for all images. The reason that lack of intensity calibration should not affect the bell-shape behavior was that the main effect of passing images through photographic media is to raise the intensities to a power (the gamma of the emulsion; Altman, 1995). According to our definition of contrast (see note 3), the effect of raising the image to a power would be to multiply the contrast by that power. Hence, from equations 3.5 and 3.6, the local-asperity error would be simply multiplied by a constant, which could be absorbed in φ_A, with no change in the bell-shape behavior (see Figure 3). To test the implications of high-frequency loss, we saved the nine Sowerby images in JPEG with the highest compression factor allowed in Photoshop (Adobe, San Jose, CA), which produced files approximately 9.5 times smaller than before compression. As before, the simulations showed the bell-shape behavior for all images. The only effect of JPEG storage was the generation of bell-shape curves with the same peak but slightly broader tuning, with the mean difference between the integrals over intensity before and after JPEG conversion being smaller than 25%. The explanation for the loss of tuning may be related to losses of contrast due to the compression algorithm (Fernandez, 1997). Loss of high-spatial frequencies would smear edges and thus cause the loss of some of them due to noise. With fewer borders, the images would be less rugged and thus lead to larger lateral-inhibition extents than if the images did not lose high frequencies (see section 4.2).

Finally, the approximations made to simulate the hypothesis may also limit the validity of the results. For instance, it would be interesting to include more realistic statistics about natural scenes (Zhu & Mumford, 1997) rather than approximate their distribution as homogeneous in our mathematical derivations (see section 3.2). Moreover, although we argue that the amplitude does not matter (see section 3.3), we could eliminate the square-function approximation for the inhibitory filter (see the appendix). Below, we will provide arguments for the bell-shape behavior that are essentially independent of the square-function assumption for the filter.

5.2 Why Does the Hypothesis Account for the Bell-Shape Behavior? We now illustrate with a simple 1D stepwise model of the image and a 1D approximation of the hypothesis what accounts for the bell-shape behavior of the lateral-inhibition extent observed in the biology. This model and the approximation simplify the mathematics and consequently will

help explain the bell-shape behavior and the meaning of the parameters involved.

The 1D image model to which we apply the new hypothesis is illustrated by the dashed line in Figure 2.2B. The model specifies the distributions of intensity (around a mean intensity) and object size (step length), but these distributions are not important here. By adding Poisson noise to the intensity, we can compute the quantal-noise and local-asperity errors needed for equation 3.3. The approximation here uses a continuum version of the image intensity and inhibitory filter. Substituting equation 3.6 for P_O in equation 3.5 and setting $\varphi_A = 1$ (see the appendix for a justification) in the 1D version of equation 3.5, we obtain

$$E_A = \sum_k \left(\sum_{i=k-\rho}^{k+\rho} \left| \frac{\nabla I}{I} \right|_i^m \right). \tag{5.1}$$

The internal sum in this 1D simplification of the model can be approximated as the sum of two terms ($E_A = E_{A_1} + E_{A_2}$). The first (E_{A_1}) is due to occluding borders (with no noise) and the second (E_{A_2}) to fluctuations caused by noise (with no occluding borders). We use a mean-field approximation for the first term, that is, we substitute the mean value of $|\frac{\nabla I}{I}|_i^m$ for its particular value at each border. In this case, if we define $\langle |\frac{\nabla I}{I}|_i^m \rangle = \Lambda / 4L$, where $\Lambda > 0$ is a constant and L is the image's size, then from equation 5.1, the first term is

$$E_{A_1} = \frac{\Lambda \rho}{2}. \tag{5.2}$$

(See Balboa, 1997, for further justification of equation 5.2.)

The second term is the quantal effect in E_A without the effect of the occluding borders. Therefore, to calculate this term, we can assume a homogeneous illumination of the retina and compute the quantal error only for the internal sum in equation 5.1 since in this case the effect of the external sum is only to insert a multiplicative constant. For the internal sum, we approximately have a variance

$$Var \left(\sum_{i=k-\rho}^{k+\rho} \left| \frac{\nabla I}{I} \right|_i^m \right) = \gamma \rho \frac{\sigma^{2m}}{\langle I_i \rangle^{2m}}, \tag{5.3}$$

where $\gamma > 0$ is a constant and σ^2 is the variance corresponding to the mean intensity $\langle I_i \rangle$ if one adds Poisson noise. The explanation for this equation is as follows: The variance of the sum of independent variables is the sum of the variances, which explains ρ. To approximate the variance of $|\frac{\nabla I}{I}|_i^m$, we can write both the numerator and denominator inside the absolute value

as a mean plus a small error, and extract the first-order term of the Taylor expansion. Because here the mean of ∇I is zero, the expansion yields the error of $|\nabla I|^m$ divided by the mean of $|I|^m$. This explains the $\langle I_i \rangle^{2m}$ term in equation 5.3 ("m" for the power of $|I|$ and "2" for the variance). Next, we need to evaluate the variance of the error of $|\nabla I|^m$. If we approximate I's Poisson noise as gaussian (not too low intensities), then the distribution of ∇I is also gaussian with zero mean and variance proportional to σ^2. Transforming such distributions to $|\nabla I|^m$ and calculating the variance (Gradshtein & Ryzhik, 1994) yields a variance proportional to σ^{2m}. This explains the σ^{2m} term in the numerator of equation 5.3. Hence, by taking the square root of this equation and remembering that for a Poisson noise, σ^2 is proportional to $\langle I_i \rangle$, the E_{A_2} error is

$$E_{A_2} = \frac{\eta \rho^{\frac{1}{2}}}{\langle I_i \rangle_x^{\frac{m}{2}}} \tag{5.4}$$

where $\eta > 0$ is a constant.

Besides these two terms of the local-asperity error (E_{A_1} and E_{A_2}), one needs the 1D quantal-noise error. To estimate this error, we use for the inhibitory filter a 1D version of the square profile defined in equation A.1 in the appendix ($\hat{h}_i = \frac{1}{2\rho}$ if $|i| \leq \rho$; 0 otherwise). Substituting this profile for $\hat{h}_i$ in equation 3.4, we obtain

$$E_Q = \frac{\varphi^*}{(\rho \langle I_i \rangle_x)^{\frac{1}{2}}}, \tag{5.5}$$

where $\varphi^* > 0$ is a constant.

The error function to minimize (the approximation of equation 3.3) is the sum of equations 5.2, 5.4, and 5.5, that is,

$$E = \frac{\Lambda \rho}{2} + \frac{\eta \rho^{1/2}}{\langle I \rangle_x^{\frac{m}{2}}} + \frac{\varphi^*}{(\rho \langle I \rangle_x)^{1/2}}. \tag{5.6}$$

To find the optimal lateral-inhibition filter, one must find the optimal ρ. From equation 5.6, the optimal ρ varies with intensity ($\langle I \rangle_x$) and the power (m) of the probability that there is an occluding border at a point as a function of its contrast. To study the dependence of the optimal ρ on intensity, one has to take the derivative of equation 5.6 with respect to ρ, equate the result to zero, and make the variable change $z = \frac{1}{\langle I \rangle_x^{1/2}}$, to obtain

$$\eta \rho z^m - \varphi^* z + \Lambda \rho^{3/2} = 0. \tag{5.7}$$

Let us first consider $m = 2$. The equation has the roots

$$z = \frac{\varphi^* \pm \sqrt{\varphi^{*2} - 4\Lambda \eta \rho^{5/2}}}{2\eta \rho}. \tag{5.8}$$

Therefore, for a sufficiently small extent ($\varphi^{*2} > 4\Lambda\eta\rho^{5/2}$), there are two intensities that minimize the error. We will now demonstrate that with the lower of these two intensities, the extent increases with intensity, while with the other one, the extent falls with intensity. Let us study the roots when $\rho \to 0$: $\varphi^{*2} > 4\Lambda\eta\rho^{5/2}$. In this case, there are two positives roots to equation 5.7.

Case 1: $z = \frac{\varphi^* + \sqrt{\varphi^{*2} - 4\Lambda\eta\rho^{5/2}}}{2\eta\rho}$ (high z corresponds to low intensity). Using the two first terms of Taylor's expansion of z with respect to $4\Lambda\eta\rho^{5/2}$, one can show

$$Lim_{\rho\to 0}\frac{\varphi^* + \sqrt{\varphi^{*2} - 4\Lambda\eta\rho^{5/2}}}{2\eta\rho} = Lim_{\rho\to 0}\frac{\varphi^* + \varphi^* - \frac{1}{2}\frac{4\Lambda\eta\rho^{5/2}}{\varphi}}{2\eta\rho} = \infty.$$

Therefore, at low intensities, z increases when ρ decreases, and thus, ρ increases with I.

Case 2: $z = \frac{\varphi^* - \sqrt{\varphi^{*2} - 4\Lambda\eta\rho^{5/2}}}{2\eta\rho}$ (low z corresponds to high intensity). At the limit, we obtain

$$Lim_{\rho\to 0}\frac{\varphi^* - \sqrt{\varphi^{*2} - 4\Lambda\eta\rho^{5/2}}}{2\eta\rho} = Lim_{\rho\to 0}\frac{\varphi^* - \varphi^* + \frac{1}{2}\frac{4\Lambda\eta\rho^{5/2}}{\varphi^*}}{2\eta\rho} = 0.$$

Therefore, at high intensities z decreases when ρ decreases, and thus, ρ decreases as I increases.

Hence, if one sets $m = 2$ on this 1D approximation, then the filter behaves with the intensity we want when minimizing the error. Furthermore, we will show that this 1D approximation accounts for essentially all the other behaviors of lateral inhibition obtained with full natural images.

To understand why the extent of the lateral-inhibition filter always falls with intensity when $m = 1$ (see Figure 4), one must consider equation 5.7. In this case,

$$z = \frac{1}{\langle I\rangle_x} = \frac{-\Lambda\rho^{3/2}}{\eta\rho - \varphi^*}, \tag{5.9}$$

where because $\langle I\rangle_x > 0$, it follows that $\eta\rho - \varphi^* < 0$. To show that ρ falls with $\langle I\rangle_x$, one takes the reciprocal of equation 5.9 and differentiates the result by ρ to get

$$\frac{d\langle I\rangle_x}{d\rho} = \frac{\eta\rho - 3\varphi^*}{2\Lambda\rho^{5/2}}.$$

Hence, because $\eta\rho - \varphi^* < 0$, then $d\langle I\rangle_x/d\rho < 0$. This inequality demonstrates that the extent of the lateral inhibition filter (ρ) falls with mean intensity ($\langle I\rangle_x$) when $m = 1$.

One can also use equation 5.7 to understand why the bell-shape behavior becomes more pronounced as m increases (see Figure 4). The only negative term in equation 5.7 (the second one) must balance the other two. Let us say that the balance occurs at some low intensity (high z). If we were to lower the intensity further, then the first term would rapidly rise if $m \geq 1$, and more so with larger m. Hence, ρ would have to fall steeply to lower the positive terms of equation 5.7 and compensate for the rise due to the first term. Consequently, the effect of raising m is to produce a faster increase of the lateral-inhibition extent as a function of intensity at low intensities.

We can also explain the increase of the lateral-inhibition extent with φ (see Figure 3) by using the 1D equation 5.7. As φ^* increases (more weight to the quantal-noise error), the negative term of equation 5.7 also increases. Therefore, ρ must rise in positive terms to balance this increase in negativity.

From the success of these results, we believe that we can use the 1D approximation in this section to explain why even when using full natural images, the new hypothesis accounts for the bell-shape behavior of lateral-inhibition extent. It turns out that this behavior arises from the dependence of the quantal-noise and local-asperity errors on intensity. Not surprisingly, if the lateral-inhibition filter were fixed, then the quantal-noise error would fall slowly as the inverse of the square root of intensity (see Figure 6 and the third term of equation 5.6). In turn, the local-asperity error would fall rapidly with intensity at low intensities (see Figure 6 and the second term of equation 5.6) and would stabilize at high intensities (see Figure 6 and the first term of equation 5.6). As a result, at low and high intensities, the local-asperity error would dominate, forcing the filter to be narrow to minimize the total error, by straddling fewer boundaries. In contrast, at intermediate intensities, the most important error would be the quantal-noise error, which would force a wide filter to reduce the total error by averaging out the noise. Why does the local-asperity error fall fast with intensity at low intensities and stabilize at high intensities? At high intensities, the quantal-noise error is negligible, and the only errors are due to the straddling of borders, which does not depend on intensity. At low intensities, the quantal-noise error is large, producing many spurious high-contrast points that reduce the chance that a true Mach band is detected as an outlier, causing local-asperity errors.

This explanation for the bell-shape behavior is in terms of the dependence of the local-asperity and quantal-noise errors on intensity. The explanation follows from the 1D analysis and its equation, 5.6. Consequently, as the analysis of this equation showed, the existence of the bell-shape behavior is independent of parameters for $m \geq 2$. In other words, no change of parameters can cause the two curves in Figure 6 to stop intersecting at two points.

5.3 Retinal Biology. To discuss whether the minimal local-asperity hypothesis is biologically plausible, we must address two issues. First, can the

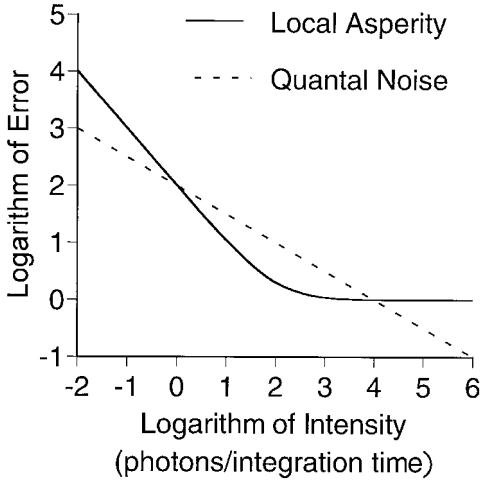

Figure 6: Relationship between the two types of errors used to compute the lateral-inhibition extent as a function of intensity. The units of intensity are arbitrary, since the curves were obtained from equation 5.6 with arbitrary choice of parameters and lateral-inhibition filter radius (ρ). The local-asperity curve corresponds to the first two terms of that equation and the quantal-noise curve to the third term. At low and high intensities, the local-asperity error dominates, but its behavior is different in each zone. This error falls fast with intensity at low intensities but is stable at high intensities. In contrast, the quantal-noise error falls steadily and slowly with intensity and dominates at intermediate intensities. When the local-asperity error dominates, the lateral-inhibition filter tends to be narrow to avoid straddling boundaries, and when the quantal-noise error dominates, the filter tends to be wide to average out the noise.

retina implement the mathematical operations specified in equations 3.4 and 3.5 to measure the error, and, relatedly, given that the postulated inhibition is nonlinear (division-like), can the retina access the image intensities or photoreceptor outputs necessary to perform these operations? Second, where in the retina are the various computations performed? What cellular mechanism does the retina use for these computations? We address the first issue elsewhere (Balboa, 1997). There, we describe simple and plausible neurophysiological mechanisms that would take care of it. We will not address it any further here, instead devoting the rest of this section to retinal-location and cellular-mechanism issues.

The minimal-local asperity hypothesis explains spatial modulations of the horizontal cell receptive field when it adapts to light intensity. There are at least four known mechanisms that could participate in this modulation. One of the mechanisms is the variation of the gap junctions between hori-

zontal cells (Mangel & Dowling, 1985; Weiler & Akopian, 1992; Myhr et al., 1994). This variation seems to be partially controlled by dopamine (Lasater & Dowling, 1985; Witkovsky & Dearry, 1991; Hampson, Weiler, & Vaney, 1994). Dopamine comes to the horizontal cell from interplexiform cells (for a review see Dowling, 1987) or by diffusion from the inner plexiform layer (Hare & Owen, 1995). In both cases, amacrine cells control the dopamine level. Therefore, the place where the retina computes the local-asperity and quantal-noise errors may be the inner plexiform layer (where amacrine cells synapse).

Another modulatory neurotransmitter system that contributes to horizontal cell coupling adaptation involves nitric oxide (NO—Miyachi, Murakami, & Nakaki, 1990; McMahon & Ponomareva, 1996; Pottek, Schultz, & Weiler, 1997). This agent appears to complement dopamine in its effects on the gap junctions (Pottek et al., 1997). Perhaps more most interesting, while NO reduces the sensitivity to glutamate of horizontal cell, dopamine increases this sensitivity (McMahon & Ponomareva, 1996). Hence, the NO system may add to the mechanism proposed here for the modulation of lateral-inhibition strength in light and dark adaptation (see Figure 5). Another such a mechanism may be the modulation of pH (Hampson et al., 1994).

A third mechanism contributing to horizontal cell adaptation involves voltage-dependent conductances in this cell (Winslow & Knapp, 1991; McMahon, 1994). In this case, the control of these conductances does not come from the inner plexiform layer (IPL), but rather from the photoreceptors. By increasing the intensity, the horizontal cells are hyperpolarized, modulating these conductances. When the conductances increase, it becomes harder to propagate current from cell to cell, therefore narrowing the receptive field of the horizontal cell (Winslow & Knapp, 1991). Because there are many types of conductances in each cell, they could contribute to a complex behavior such as the bell-shape behavior of the lateral-inhibition extent as a function of intensity.

The last mechanism that we will discuss for lateral-inhibition adaptation is a specialization of teleost fish. For these animals, increasing the intensity causes the horizontal cell to send finger-like processes to the pedicles of cones. These processes, which are called spinules (Wagner, 1980; De Juan, Iñíguez, & Dowling, 1991; Weiler & Janssen-Bienhold, 1993), increase the area of contact between the cells, and thus spinules can increase the feedback strength in the OPL. It is interesting that the control of spinule growth is partially through extraretinal efferent fibers (De Juan, García, & Cuenca, 1996; De Juan & García, 1998). This suggests that an extraretinal structure may implement some of the computations of our hypothesis in teleost fish. In particular, the external sums in equation 3.5 to estimate the local-asperity error require a computation over the entire retina, and therefore may require an integration over larger distances than available in retinal processes.

5.4 Multiple Tasks. Is lateral inhibition in the inner plexiform layer, extraretinal parts of the brain, or invertebrates doing a different thing from that in the OPL? We ask this question because other lateral-inhibition models fit well data from these systems (Srinivasan et al., 1982; Atick & Redlich, 1992). It is possible and likely that these systems use lateral inhibition for different tasks. These tasks may include extraction of different visual attributes such as direction of motion (Barlow & Levick, 1965), orientation of edges (Silito, 1975, 1979), and temporal modulation of intensity (Werblin, Maguire, Lukasiewicz, Eliasof, & Wu, 1988). And because these tasks are different, they may require different mechanisms of lateral inhibition, as observed experimentally (Merwine et al., 1995; Cook & McReynolds, 1998). These differences may explain why lateral inhibition of ganglion cells may not display a bell-shape behavior (Van Ness & Bouman, 1967). Similarly, lateral inhibition in insects does not appear to have a bell-shape behavior, since one can account for the properties of this inhibition with the predictive-coding theory (Srinivasan et al., 1982; van Hateren, 1992; Balboa & Grzywacz, 2000). Why would the tasks be different in insects? Perhaps the answer is that their "retina" must achieve in one or two layers many of the goals of several layers of the vertebrate system. Moreover, the brains of insects are much smaller than those of vertebrates, making neural resources more constraining (Brooke, Hanley, & Laughlin, 1998) and thus forcing "careful consideration" of tasks. Our philosophy is that for each system one must analyze tasks, limitations, and internal knowledge. There is no reason to believe that these factors are identical across systems, therefore allowing for different behavior in different systems.

Appendix

The first section of this appendix describes the computational approximations performed to implement the minimal local-Asperity hypothesis. The second section describes the error-minimization procedure and the choice of the parameters.

A.1 Approximations in the Error Estimation.

A.1.1. Approximation for the Lateral-Inhibition Filter. To simplify the computation of $h_{i,j}$ from the properties of $P_O(|\nabla I/I|_{i,j})$ (see equation 3.5) and the quantal noise (see equation 3.4), we approximate $h_{i,j}$ with a step (square) function. In other words, we use a disk in two dimensions defined as

$$\hat{h}_{i,j} = \begin{cases} \frac{1}{\pi\rho^{*2}} & \text{if } (i^2 + j^2)^{1/2} \le \rho^* \\ 0 & \text{otherwise.} \end{cases} \tag{A.1}$$

From this approximation, the radius ρ in equation 3.5 is $\rho = \rho^*/2$.

A.1.2 Approximation for $|\frac{\nabla I}{I}|_{i,j}$. The discrete approximation for the absolute value of the intensity's gradient used in the simulations is

$$|\nabla I|_{i,j} = \left(\frac{(I_{i+1,j} - I_{i-1,j})^2}{\triangle x^2} + \frac{(I_{i,j+1} - I_{i,j-1})^2}{\triangle y^2} \right)^{\frac{1}{2}},$$

where $\triangle x = \triangle y$ are the distance between neighbor pixels. Without loss of generality, we set to $\triangle x = \triangle y = 1$. Because we have to calculate $|\frac{\nabla I}{I}|_{i,j}$, we estimate the local intensity as

$$I_{i,j} = \frac{I_{i,j+1} + I_{i,j-1} + I_{i+1,j} + I_{i-1,j}}{4},$$

to reduce the effect of noise. When $I_{i,j+1} = I_{i,j-1} = I_{i+1,j} = I_{i-1,j} = 0$, there is a problem with the computation of $\frac{\nabla I}{I}$. We assume that this occurs at very dim intensities, such that the probability of each photoreceptor's absorbing a photon is small but not zero. One can approximate this case as if one of the photoreceptors absorbs a photon but the others do not. Therefore, approximately,

$$\left| \frac{\nabla I}{I} \right|_{i,j} = \left(\frac{1}{2^2} \left(\frac{4}{1} \right)^2 \right)^{\frac{1}{2}} = 2,$$

if the four values are zero. We justify this approximation by noting that if we wait a sufficiently long time, some photons will be absorbed, but the probability of absorbing more than one photon in the integration time of the four photoreceptors is very small.

A.2 Optimal Lateral-Inhibition Extent.

A.2.1 Error-Minimization Process. The program has to find the lateral-inhibition extent ($\rho = \rho^*/2$; see equations 3.4, 3.5, and A.1) that minimizes equation 3.3. The inputs to the program are the natural image, the mean intensity, and the parameters (see the next section). The program first adds noise to the image (Balboa & Grzywacz, 2000) and then computes $|\frac{\nabla I}{I}|_{i,j}$. Next, the program plugs $|\frac{\nabla I}{I}|^m_{i,j}$ into equation 3.6, uses it to calculate equation 3.5, and with the aid of this equation and equation 3.4 minimizes equation 3.3. The minimization procedure is by exhaustive search over ρ in geometric steps of 2, starting at 2 pixels. After completion of the exhaustive search, the program estimates the minimal ρ through interpolation with a parabola around the minimum. We use a parabola as the simplest polynomial interpolation (Burden & Faires, 1989). This minimization was performed in the $[10^{-1}, 10^6]$ range of intensities in steps of 0.5 log units.

A.2.2. Parameters. There are four parameters in the equations (n, φ_Q, φ_A, and m), but they are not all independent. Because the parameters φ_Q and φ_A weigh two terms whose sum is to be minimized, these parameters are not independent. Multiplying them by a common factor does not change the minimizing filter. Hence, without loss of generality, we set the parameter $\varphi_A = 1$. We also define the parameter $\varphi = \varphi_Q/(2\pi^{1/2})$ so that for the filter in equation A.1, E_Q has the simple form $E_Q = \varphi/\rho\langle I\rangle^{1/2}$. Thus, the only true free parameters are n, φ, and m. To learn their effects on the theory, we vary them in the ranges [1, 3], [100, 10,000], and [1, 4], respectively, in the simulations.

Acknowledgments

We thank Stewart Bloomfield for sending us his data on horizontal cell adaptation before publication and Alexander Ball for loaning us his only copy of Jamieson's doctoral dissertation. Thanks are also due to Andrew Wright for allowing us to use the Sowerby Image Database (British Aerospace) and to Alan Yuille and Scott Konishi for sharing with us their TIFF version of the images from this database. We thank Joaquín De Juan, Russell Hamer, and the reviewers of this article for critical comments. Alan Yuille, Pierre-Ives Burgi, and Davi Geiger wrote letters of support for R.B.'s work before it was defended as a thesis in computer science. Finally, we thank José Oncina for financial support during R.B.'s Ph.D. work at the University of Alicante, Alicante, Spain. This work was supported by National Eye Institute grants EY08921 and EY11170 and the William A. Kettlewell Chair to N.M.G., by Grant TIC97-0941 to Dr. José Oncina, and by a National Eye Institute Core grant to Smith-Kettlewell.

References

Adelson, E. H. (1993). Perceptual organization and the judgment of brightness. *Science, 262*, 2042–2044.

Altman, J. H. (1995). Photographic films. In M. Bass (Ed.), *Handbook of optics, Vol. 1: Fundamentals, techniques and design*. New York: McGraw-Hill.

Ammermüller, J., Muller, J. F., & Kolb, H. (1995). The organization of the turtle inner retina. II. Analysis of color-coded and directionally selective cells. *J. Comp. Neurol., 358*, 35–62.

Ashmore, J. F., & Falk, G. (1980). The single-photon signal in rod bipolar cells of the dogfish retina. *J. Physiol. Lond., 300*, 151–166.

Atick, J. J., & Redlich, A. N. (1992). What does the retina know about natural scenes? *Neural Comp., 4*, 196–210.

Balboa, R. M. (1997). *Teorías para la inhibición lateral en la retina basadas en autocorrelación, curtosis y aspereza local de las imágenes naturales*. Unpublished doctoral dissertation, University of Alicante, Alicante, Spain.

Balboa, R. M., & Grzywacz, N. M. (1998). The minimal-local asperity theory of retinal lateral inhibition. *Invest. Ophthalmol. Vis. Sci., 39*, S562.

Balboa, R. M. & Grzywacz, N. M. (1999a). *Occlusions contribute to scaling in natural images*. Manuscript submitted for publication.

Balboa, R. M., & Grzywacz, N. M. (1999b). *Occulusions and their relationship with the distribution of contrasts in natural images*. Manuscript submitted for publication.

Balboa, R. M., & Grzywacz, N. M. (1999c). Biological evidence for an ecological-based theory of early retinal lateral inhibition. *Invest. Ophthalmol. Vis. Sci., 40*, S386.

Balboa, R. M., & Grzywacz, N. M. (2000). The role of early retinal lateral inhibition: More than maximizing luminance information. *Vis. Neurosci., 17:1*.

Baldridge, W. H. (1993). *Effect of background illumination on horizontal cell receptive-field size in the retina of the goldfish* (*Carassius auratus*). Unpublished doctoral dissertation. McMaster University, Hamilton, Ontario, Canada.

Baldridge, W. H., & Ball, A. K. (1991). Background illumination reduces horizontal cell receptive field size in both normal and 6-hydroxydopamine-lesioned goldfish retinas. *Visual Neurosci., 7*, 441–450.

Barlow, H. B., Fitzhugh, R., & Kuffler, S. W. (1957). Change of organisation in the receptive fields of the cat's retina during dark adaptation. *J. Physiol., 137*, 338–354.

Barlow, H. B., & Levick, W. R. (1965). The mechanism of directionally selective units in the rabbit's retina. *J. Physiol., 178*, 477–504.

Bartlett, M. S., & Sejnowski, T. J. (1998). Learning viewpoint-invariant face representations from visual experience in an attractor network. *Network, 9*, 399–417.

Baylor, D. A., Lamb, T. D., & Yau, K.-W. (1979). Responses of retinal rods to single photons. *J. Physiol., 288*, 613–634.

Berger, J. O. (1985). *Statistical decision theory and Bayesian analysis*. New York: Springer-Verlag.

Bowling, D. B. (1980). Light responses of ganglions cells in the retina of the turtle. *J. Physiol., 209*, 173–196.

Brooke, M. de L., Hanley, S., & Laughlin, S. B. (1998). The scaling of eye size with body mass in birds. *Proc. R. Soc. Lond. B, 266*, 405–412.

Burden, R. L., & Faires, J. D. (1989). *Numerical analysis* (4th ed.). Boston: PWS-KENT Publishing Company.

Burington, R. S. (1973). *Handbook of mathematical tables and formulas*. New York: McGraw-Hill.

Calkins, D. J., & Sterling, P. (1996). Absence of spectrally specific lateral inputs to midget ganglion cells in primate retina. *Nature, 381*(6583), 613–615.

Campbell, F. W., & Robson, J. G. (1968). Application of Fourier analysis to the visibility of gratings. *J. Physiol. (Lond.), 197*, 551–566.

Cook, P. B., & McReynolds, J. S. (1998). Modulation of sustained and transient lateral inhibitory mechanisms in the mudpuppy retina during light adaptation. *J. Neurophysiol., 79*, 197–204.

Dacey, D. M. (1996). Circuitry for color coding in the primate retina. *Proc. Natl. Acad. Sci. USA, 93*, 582–588.

De Juan, J., & García, M. (1998). Interocular effect of actin depolymerization on spinule formation in teleost retina. *Brain Res., 792*, 173–177.

De Juan, J., García, M., & Cuenca, N. (1996). Formation and dissolution of spinules and changes in nematosome size require optic nerve integrity in black bass (*Micropterus salmoides*) retina. *Brain Res., 707*, 213–220.

De Juan, J., Iñíguez, C., & Dowling, J. E. (1991). Nematosomes in external horizontal cells of white perch (*Roccus americana*) retina: Changes during dark and light adaptation. *Brain Res., 546*, 176–180.

Dowling, J. E. (1987). *The retina: An approachable part of the brain*. Cambridge, MA: Belknap Press of Harvard University Press.

Fain, G., & Dowling, J. E. (1973). Intracellular recordings from single rods and cones in the mudpuppy retina. *Science, 180*, 1178–1181.

Fernandez, J. N. (1997). *GIFs, JPEGs and BMPs: Handling Internet graphics*. Cambridge, MA: MIT Press.

Field, D. J. (1994). What is the goal of sensory coding? *Neural Comp., 6*, 559–601.

Fiorentini, A., & Radici, T. (1957). Binocular measurements of brightness on a field presenting a luminance gradient. *Atti. Fond. Giorgio Ronchi, XII*, 453–461.

Fuortes, M. G. F., & Yeandle, S. (1964). Probability of occurrence of discrete potentials waves in the eye of the *Limulus*. *J. Physiol., 47*, 443–463.

Gallant, S. I. (1995). Expert systems and decision systems using neural networks. In M. A. Arbib, (Ed.), *The handbook of brain theory and neural networks* (pp. 377-389). Cambridge, MA: MIT Press.

Gradshtein, I. S., & Ryzhik, I. M. (1994). *Table of integrals, series, and products* (5th ed.). San Diego, CA: Academic Press.

Grzywacz, N. M., & Balboa, R. M. (1999). *The minimal-local asperity theory of early retinal lateral inhibition*. Manuscript submitted for publication.

Grzywacz, N. M., & Hillman, P. (1988). Biophysical evidence that light adaptation in *Limulus* photoreceptors is due to a negative feedback. *Biophys. J., 53*, 337–348.

Grzywacz, N. M., Hillman, P., & Knight, B. W. (1988). The quantal source of area supralinearity of flash responses in *Limulus* photoreceptors. *J. Gen. Physiol., 91*, 659–684.

Hampson, E. C., Weiler, R., & Vaney, D. I. (1994). pH-gated dopaminergic modulation of horizontal cell gap junctions in mammalian retina. *Proc. R. Soc. Lond. B., 255*, 67–72.

Hare, W. A., & Owen, W. G. (1995). Similar effects of carbachol and dopamine on neurons in the distal retina of the tiger salamander. *Vis. Neurosci., 12*, 443–455.

Jamieson, M. S. (1994). *Mechanisms regulating horizontal cell receptive field size in goldfish retina*. Unpublished doctoral dissertation, McMaster University, Hamilton, Ontario, Canada.

Jamieson, M. S., Baldridge, W. H., & Ball, A. K. (1994). Modulation of horizontal cell receptive field size in light-adapted godlfish retinas. In *Proceedings of the Association for Research in Vision and Ophthalmology* (pp. 1821, 2623).

Jones, M. J., Sinha, P., Vetter, T., & Poggio, T. (1997). Top-down learning of low-level vision tasks. *Curr. Biol., 7*, 991–994.

Kamermans, M., Haak, J., Habraken, J. B., & Spekreijse, H. (1996). The size of the horizontal cell receptive fields adapts to the stimulus in the light adapted goldfish retina. *Vision Res., 36*, 4105–4119.

Kamermans, M., Kraaij, D. A., & Spekreijse, H. (1998). The cone/horizontal cell network: A possible site for color constancy. *Vis. Neurosci., 15*, 787–797.

Lankheet, M. J., Rowe, M. H., Van Wezel, R. J., & van de Grind, W. A. (1996). Spatial and temporal properties of cat horizontal cells after prolonged dark adaptation. *Vision Res., 36*, 3955–3967.

Lasater, E. M., & Dowling, J. E. (1985). Dopamine decreases conductance of the electrical junctions between cultured retinal horizontal cells. *Proc. Natl. Acad. Sci. USA, 82*, 3025–3029.

Lillywhite, P. G. (1977). Single photon signals and transduction in an insect eye. *Journal of Comparative Physiology, 122*, 189–200.

Mackeown, W. P. J. (1994). *Labelling image database and its application to outdoor scene analysis*. Unpublished doctoral dissertation, University of Bristol.

Mangel, S. C., & Dowling, J. E. (1985). Responsiveness and receptive field size of carp horizontal cells are reduced by prolonged darkness and dopamine. *Science, 229*, 1107–1109.

McCarthy, S. T., & Owen, W. G. (1996). Preferential representation of natural scenes in the salamander retina. *Invest. Ophthalmol. Vis. Sci., 37*, S674.

McMahon, D. G. (1994). Modulation of electrical synaptic transmission in zebrafish retinal horizontal cells. *J. Neurosci., 14*, 1722–1734.

McMahon, D. G., & Ponomareva, L. V. (1996). Nitric oxide and cGMP modulate retinal glutamate receptors. *J. Neurophysiol., 76*, 2307–2315.

Merwine, D. K., Amthor, F. R., & Grzywacz, N. M. (1995). Interaction between center and surround in rabbit retinal ganglion cells. *J. Neurophysiol., 73*, 1547–1567.

Miyachi, E., Murakami, M., & Nakaki, T. (1990). Arginine blocks gap junctions between retinal horizontal cells. *Neuroreport, 1*, 107–110.

Mobley, C. (1995). Optical properties of water. In M. Bass (Ed.), *Handbook of optics, Vol. 1: Fundamentals, techniques and design*. New York: McGraw-Hill.

Myhr, K. L., Dong, C. J., & McReynolds, J. S. (1994). Cones contribute to light-evoked, dopamine-mediated uncoupling of horizontal cells in the mud-puppy retina. *J. Neurophysiol., 72*, 56–62.

Ogden, T. E., Mascetti, G. G., & Pierantoni, R. (1985). The outer horizontal cell of the frog retina: Morphology, receptor input, and function. *Invest. Ophthalmol. Vis. Sci., 26*, 643–656.

Pottek, M., Schultz, K., & Weiler, R. (1997). Effects of nitric oxide on the horizontal cell network and dopamine release in the carp retina. *Vision Res., 37*, 1091–1102.

Rao, R., Buchsbaum, G., & Sterling, P. (1994). Rate of quantal transmitter release at the mammalian rod synapse. *J. Biophys., 67*, 57–63.

Ratliff, F. (1965). *Mach bands: Quantitative studies on neural networks in the retina*. San Francisco: Holden-Day.

Reifsnider, E. S., & Tranchina, D. (1995). Background contrast modulates kinetics and lateral spread of responses to superimposed stimuli in outer retina. *Vis. Neurosci., 12*, 1105–1126.

Ridley, M. (1993). *Evolution*. Boston: Blackwell Scientific.

Robson, J. G., & Frishman L. J. (1995). Response linearity and kinetics of the cat retina: The bipolar cell component of the dark-adapted electroretinogram. *Vis. Neurosci., 12*, 837–850.

Rodiek, R. W., & Stone, J. (1965). Analysis of receptive fields of cat retinal ganglion cells. *J. Neurophysiol., 28*, 832–849.

Ruderman, D. L., & Bialek, W. (1994). Statistics of natural images: Scaling in the woods. *Phys. Rev. Letter, 73*, 814–817.

Rushton, W. A. H. (1961). The intensity factor in vision. In W. D. McElroy & H. B. Glass (Eds.), *Light and Life* (pp. 706–722). Baltimore: Johns Hopkins University Press.

Shapley, R. M., & Tolhurst, D. J. (1973). Edge-detectors in human vision. *J. Physiol. (Lond.), 229*, 165–183.

Silito, A. M. (1975). The contribution of inhibitory mechanisms to the receptive field properties of neurones in the striate cortex of the cat. *J. Physiol. (Lond.), 250*, 305–322.

Silito, A. M. (1979). Inhibitory mechanisms influencing complex cell orientation selectivity and their modification at high resting discharge levels. *J. Physiol. (Lond.) 289*, 33–53.

Srinivasan, M. V., Laughlin, S. B., & Dubs, A. (1982). Predictive coding: A fresh view of inhibition in the retina. *Proc. R. Soc. Lond. B., 216*, 427–459.

Stevens, S. S. (1970). Neural events and the psychophysical law. *Science, 170*, 1043–1050.

Tranchina, D., Gordon, J., Shapley, R., & Toyoda, J. (1981). Linear information processing in the retina: A study of horizontal cell responses. *Proc. Natl. Acad. Sci. USA, 78*, 6540–6542.

van Hateren, J. H. (1992). Theoretical predictions of spatiotemporal receptive fields of fly LMC's, and experimental validation. *J. Comp. Physiol. A, 171*, 157–170.

Van Ness, F. L., & Bouman, M. A. (1967). Spatial modulation transfer in the human eye. *J. Opt. Soc. Am., 57*, 401–406.

Verweij, J., Kamermans, M., & Spekreijse, H. (1996). Horizontal cells feed back to cones by shifting the cone calcium-current activation range. *Vision Res., 36*(24), 3943–3953.

Verweij, J., Kamermans, M., van den Aker, E. C., & Spekreijse, H. (1996). Modulation of horizontal cell receptive fields in the light adapted goldfish retina. *Vision Res., 36*, 3913–3923.

Vu, T. Q., McCarthy, S. T., & Owen, W. G. (1997). Linear transduction of natural stimuli by dark-adapted and light-adapted rods of the salamander, it Ambystoma tigrinum. *J. Physiol., 505*, 193–204.

Wagner, H. J. (1980). Light-dependent plasticity of the morphology of horizontal cell terminals in cone pedicles of fish retinas. *J. Neurocytol., 9*, 573–590.

Weiler, R., & Akopian, A. (1992). Effects of background illuminations on the receptive field size of horizontal cells in the turtle retina are mediated by

dopamine. *Neurosci. Lett., 140*, 121–124.
Weiler, R., & Janssen-Bienhold, U. (1993). Spinule-type neurite outgrowth from horizontal cells during light adaptation in the carp retina: An actin-dependent process. *J. Neurocytol., 22*, 129–139.
Weiss, Y., Edelman, S., & Fahle, M. (1993). Models of perceptual learning in vernier hyperacuity. *Neural Comp., 5*, 695–718.
Werblin, F. S. (1977). Synaptic interactions mediating bipolar response in the retina of the tiger salamander. In H. B. Barlow and P. Fatt (Eds.), *Vertebrate Photoreception* (pp. 205–230). San Diego, CA: Academic Press.
Werblin, F. S., Maguire, G., Lukasiewicz, P., Eliasof, S., & Wu, S. M. (1988). Neural interactions mediating the detection of motion in the retina of the tiger salamander. *Vis. Neurosci., 1*, 317–329.
Winslow, R. L., & Knapp, A. G. (1991). Dynamic models of the retinal horizontal cell network. *Prog. Biophys. Mol. Biol., 56*, 107–133.
Wishart, K. A., Frisby, J. P., & Buckley, D. (1997). The role of 3-D surface slope in a lightness/brightness effect. *Vis. Res., 37*, 467–473.
Witkovsky, P., & Dearry, A. (1991) Functional roles of dopamine in the vertebrate retina. *Prog. Ret. Res., 11*, 247–292.
Xin, D., & Bloomfield, S. A. (1999). Dark- and light-induced changes in coupling between horizontal cells in mammalian retina. *J. Comp. Neurol., 405*, 75–87.
Xin, D., Bloomfield, S. A., & Persky, S. E. (1994). Effect of background illumination on receptive field and tracer-coupling size of horizontal cells and AII amacrine cells in the rabbit retinas. In *Proceedings of the Association for Research in Vision and Ophthalmology* (p. 1363).
Zhu, S. C., & Mumford, D. (1997). Prior learning and Gibbs reaction-diffusion. *IEEE Trans. on Pattern Analysis and Machine Intelligence, 19*, 1236–1250.
Zhu, S. C., & Mumford, D. (1998). GRADE: Gibbs reaction and diffusion equations. A framework for pattern synthesis, image denoising, and removing clutter. In *Proceedings of the 6th International Conference on Computer Vision* (pp. 847–854).

Received October 21, 1998; accepted August 6, 1999.